

Journal Pre-proofs

Substituted pyridine-quinoline ligands as building blocks for neutral rhodium(III) complexes. Synthesis, structural characterization studies and anti-platelet activity towards the Platelet-Activating Factor (PAF)

Antigoni Margariti, Vasiliki D. Papakonstantinou, George M. Stamatakis, Constantinos A. Demopoulos, Gregor Schnakenburg, Aikaterini K. Andreopoulou, Panagiotis Giannopoulos, Joannis K. Kallitsis, Athanassios I. Philippopoulos

PII: S0277-5387(19)30781-8
DOI: <https://doi.org/10.1016/j.poly.2019.114336>
Reference: POLY 114336

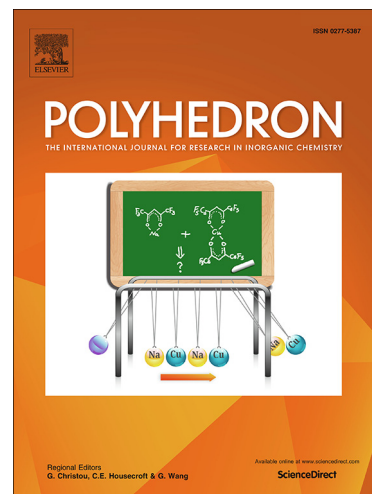
To appear in: *Polyhedron*

Received Date: 5 December 2019
Revised Date: 23 December 2019
Accepted Date: 27 December 2019

Please cite this article as: A. Margariti, V.D. Papakonstantinou, G.M. Stamatakis, C.A. Demopoulos, G. Schnakenburg, A.K. Andreopoulou, P. Giannopoulos, J.K. Kallitsis, A.I. Philippopoulos, Substituted pyridine-quinoline ligands as building blocks for neutral rhodium(III) complexes. Synthesis, structural characterization studies and anti-platelet activity towards the Platelet-Activating Factor (PAF), *Polyhedron* (2019), doi: <https://doi.org/10.1016/j.poly.2019.114336>

This is a PDF file of an article that has undergone enhancements after acceptance, such as the addition of a cover page and metadata, and formatting for readability, but it is not yet the definitive version of record. This version will undergo additional copyediting, typesetting and review before it is published in its final form, but we are providing this version to give early visibility of the article. Please note that, during the production process, errors may be discovered which could affect the content, and all legal disclaimers that apply to the journal pertain.

© 2019 Elsevier Ltd. All rights reserved.



Substituted pyridine-quinoline ligands as building blocks for neutral rhodium(III) complexes. Synthesis, structural characterization studies and anti-platelet activity towards the Platelet-Activating Factor (PAF)

Antigoni Margariti,^a Vasiliki D. Papakonstantinou,^b George M. Stamatakis,^b Constantinos A. Demopoulos,^b Gregor Schnakenburg,^c Aikaterini K. Andreopoulou,^d Panagiotis Giannopoulos,^d Joannis K. Kallitsis,^d and Athanassios I. Philippopoulos,^{*a}

^a *Laboratory of Inorganic Chemistry, Department of Chemistry, National and Kapodistrian University of Athens, Panepistimiopolis Zografou 15771, Athens, Greece*

^b *Laboratory of Biochemistry, Department of Chemistry, National and Kapodistrian University of Athens, Athens 15771, Greece*

^c *Institut für Anorganische Chemie, Rheinische Friedrich-Wilhelms-Universität Bonn, Gerhard-Domagk-Straße 1, D-53121 Bonn, Germany*

^d *Department of Chemistry, University of Patras, 26504, Patras, Greece*

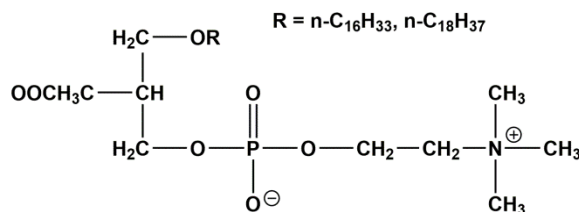
* Corresponding Author: Athanassios I. Philippopoulos Tel: +30-210-7274697, Fax: +30-210-7274782, Email: atphilip@chem.uoa.gr

Abstract

The Friedländer condensation reaction was employed to synthesize the new bidentate ligands namely 6-bromo-4-phenyl-2-pyridin-2-yl-quinoline (**1**) and 4-(4-phenyl-2-(pyridin-2-yl)quinolin-6-yl)phenol (**2**). These compounds were fully characterized including the X-ray structures of **1** and the protonated form of **2**, i.e. **2**·HCl·H₂O. We also report the synthesis and spectroscopic characterization of two rhodium(III) complexes of the general formula [Rh(**1**)Cl₃(CH₃OH)] (**3**) and [Rh(**2**)Cl₃(CH₃OH)] (**4**). The molecular structures of **3**·2CH₃OH and **4** were determined by single-crystal X-ray diffraction studies, revealing that these complexes adopt the *mer*-configuration. The solution stability of **3**, **4** was studied by a combination of UV-Vis and ¹H NMR spectroscopic techniques. All compounds were biologically evaluated for their anti-platelet activity using their potency to inhibit the action of PAF (Platelet-Activating Factor), which is an approach of continuous interest in the field. Complexes **3** and **4** were found to be potent PAF inhibitors with IC₅₀ values in the micromolar range (1.0 μM and 3.9 μM respectively). Since PAF is the most potent inflammatory lipid mediator, the PAF-inhibitors and consequently the title compounds may be considered as potent examples in the search for novel anti-inflammatory drugs.

1. Introduction

Platelet-Activating Factor (PAF) is the most potent inflammatory lipid mediator that participates in a wide range of pathophysiological actions (Scheme 1). Its systematic name has been identified as 1-O-alkyl-2-acetyl-*sn*-glycero-3-phosphocholine [1] however the term PAF includes a broader group of structurally related (or not related) lipids sharing PAF-like activity [2].



Scheme 1. The molecular structure of PAF

The biological activity of PAF is achieved through binding to a G-protein coupled receptor found on the plasma membrane of cells or intracellular membranes [3]. As a result, the interaction between PAF and PAFR (PAF-receptor) initiates a cascade of intracellular signaling pathways, cell/species- dependent, which convert the mediator's message to a final cell response [3].

As far as the PAF inhibitors are concerned there is a wide range of compounds that generally are divided into two categories: the non-specific and the specific PAF inhibitors [3,4]. The latter (specific PAF inhibitors) constitute a special class of either naturally occurring compounds such as Gingolides [2,5] or synthetically prepared ones like rupatadine fumarate [2,6] that antagonize competitively or noncompetitively, the binding of PAF to its receptor.

Although, organic PAF antagonists exist [3,7], reports on analogous metal-based inhibitors of PAF are quite rare [3]. This is surprising taking into consideration the numerous advantages of metal-based therapeutics addressed over the organic analogues [8,9,10]. In addition the role of metal complexes in inorganic medicinal chemistry has been well documented [11,12].

Our interest to investigate the area of metal-based complexes as potential anti-PAF agents (anti-inflammatory action) stems from the fact that in general metal-based inhibitors of biological probes, constitute a vast research area owing to the remarkable characteristics of the metal ions like structural diversity, redox behavior, the possibility of tuning thermodynamic and kinetic ligand substitution etc. [3,13].

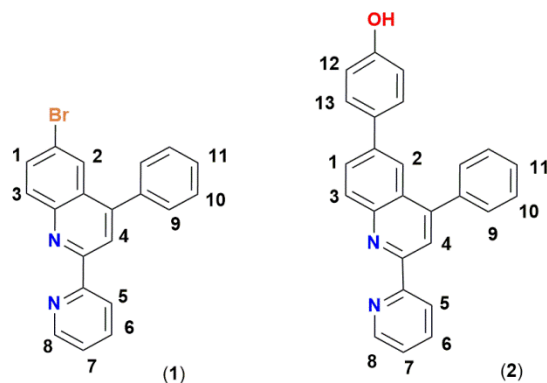
Intrigued by these challenges a systematic approach has been initiated towards the preparation of potent metal-based inhibitors of PAF, mainly transition metal complexes. Since PAF is a potent mediator of inflammation, inhibition of its biological activity (anti-PAF action) by metal-based inhibitors, could contribute to the

development of new agents that may have potential anti-inflammatory effects. Notably, this an approach of continuous interest, as clearly demonstrated from our contributions in the area, including a series of very effective rhodium [14–17], iridium [18] and ruthenium based inhibitors [19,20] of PAF with nanomolar and sub-micromolar activity. Recent results in this topic have been summarized on a review paper and a book chapter contribution [3,17] and by other research groups [21,22].

The well expressed anti-platelet activity of rhodium(I) and rhodium(III) complexes bearing quinoxaline and carboxy-pyridine quinoline ligands [15] prompted us so as to further explore the inhibitory effect of new bifunctional organic ligands against the PAF-induced aggregation. Substituted pyridine-quinoline ligands, constitute the basis of this work since (i) their chemistry is closely related to that of the ligands described in our previous publications [14,15] and (ii) the number of known metal complexes with this class of organic substances is limited [23,24,25]. In addition, the knowledge that could be obtained from such study could be evaluated further and contribute to the structure-activity relationship developed [3,17].

For this purpose, two substituted pyridine-quinoline based ligands, namely the 6-bromo-4-phenyl-2-pyridin-2-yl-quinoline (**1**) and the 4-(4-phenyl-2-(pyridin-2-yl)quinolin-6-yl)phenol (**2**) were designed and the coordination chemistry of **1**, **2** to a rhodium(III) center was investigated (Scheme 2). Accordingly, the synthesis and complete characterization of the new versatile chelating ligands **1**, **2** and their rhodium(III) complexes *mer*-[Rh(**1**)Cl₃(CH₃OH)] (**3**) and *mer*-[Rh(**2**)Cl₃(CH₃OH)] (**4**) is described. Such a synthetic procedure allows us to study the properties of the new complexes and evaluate the influence of the organic moieties on the biological activity measured.

In addition, in this manuscript we report for the first time, on the *in vitro* biological activity (anti-PAF action) of this category of ligands and of their relevant rhodium(III) coordination compounds. The inhibitory effect of the new substances was studied on PAF-induced platelet aggregation toward washed rabbit platelets (WRPs).



Scheme 2. Structures of ligands **1** and **2** and atom labeling for NMR assignments.

2. Materials and methods

2.1. Reagents and equipments

$\text{RhCl}_3 \times 3\text{H}_2\text{O}$ was purchased from Johnson Matthey Co. and all other reagents and solvents from Sigma Aldrich, Alfa Aesar or Acros Organics and were used without further purification unless otherwise stated. THF was dried over Na/benzophenone and distilled under argon. (2-Amino-5-bromophenyl)phenyl-methanone [26,27], 4-(tetrahydro-2H-pyran-2-yloxy) phenyl boronic acid [28], and $\text{Pd}(\text{PPh}_3)_4$ [29] were synthesized according to the literature reports. The preparation of the organic precursors **1** and **2** was performed under argon atmosphere, while the synthesis of the metal complexes **3** and **4** was carried out under aerobic conditions.

Infrared spectra were measured on a Shimadzu IR Affinity-1 spectrometer as potassium bromide pellets in the spectral range of $4000\text{--}400\text{ cm}^{-1}$. The following abbreviations were used for the intensities of the IR absorption bands: vs = very strong, s = strong, m = medium, w = weak, br = broad. Elemental analyses were obtained from the Microanalysis Center of the Institut für Anorganische Chemie Universität Bonn and from the Instrumental Analysis Laboratory of the University of Patras using a Carlo Erba CHNS-O EA1108 Elemental Analyser. ^1H NMR and ^{13}C NMR spectra were recorded at 298 K on a Varian 300 MHz and on a Bruker Advance DPX spectrometers at 400.13 (^1H NMR), and 100.6 MHz (^{13}C NMR) in CDCl_3 (containing TMS as internal standard) and in DMSO-d_6 . J values are given in Hz. The following abbreviations were used for the signal multiplicities: s = singlet, d = doublet, t = triplet, m = multiplet, br

= broad. Absorption spectra were recorded with a CARY 3E UV-Vis spectrometer in DMSO (DMSO = (CH₃)₂SO) solution. Mass spectra were recorded on a Waters Acquity ESI-MS system with a Waters 2966 Photodiode Array detector coupled to a Waters Micromass ZQ mass spectrometer. A single-quadrupole Quattro micro mass spectrometer (ACQUITY SQ Detector) equipped with an electrospray ionization (ESI) interface was used for analytical detection. ESI-MS was operated in positive mode under the following operating parameters: capillary voltage, 3.5 kV; cone voltage, 30 V; source temperature, 80 °C; desolvation temperature, 300 °C; desolvation gas (nitrogen), 5500 L/h; cone gas (nitrogen), 50 L/h. All data were acquired and processed using Masslynx 4.1 software (Waters Corp., MA, Milford, USA). Melting or decomposition points were determined using an Electrothermal 9100 (IA9000 series) Digital melting point apparatus and are uncorrected. The samples were sealed in capillary tubes and heated slowly until the compounds melted or decomposed. Thermal stability studies were performed with a Thermal analysis Mettler/Toledo TGA/DSC system under nitrogen atmosphere, between temperature range 25–800 °C and with a temperature increase rate of 10 °C/sec.

2.2. Synthetic procedure and spectral data

2.2.1. Synthesis of 6-bromo-4-phenyl-2-pyridin-2-yl-quinoline (1)

Into a 50 mL round bottom flask and under a slow stream of argon, 2-amino-5-bromophenyl(phenyl)methadone (3 g, 10.86 mmol) and acetylpyridine (2.63 g, 21.72 mmol) were dissolved in a mixture of acetic acid (35 mL) and sulfuric acid 95% (0.1 mL). The reaction mixture was heated under reflux for 3 days. After cooling to room temperature, the brown solid precipitated was filtered off, washed repeatedly with methanol and dried under vacuum overnight. Yield: 86% (3.37 g). M.p.: 170.9–173.8 °C. *Anal.* Calc. for C₂₀H₁₃N₂Br: C, 66.50; H, 3.63; N, 7.75. Found: C, 66.47; H, 3.68; N, 7.85%. IR (KBr, $\tilde{\nu}$ in cm⁻¹): 3052 (w, ν (C–H_{arom})), 1598 (s, ν (C=C)), 1547 (m), 1529 (s), 1487 (s, ν (C=N)), 1452 (m), 1227 (w), 1117 (vs, ν_s (C–Br)), 1064 (m), 976 (w), 883 (m), 833 (m), 800 (m), 780 (m), 755 (m), 700 (s), 619 (s), 600 (w), 576 (w). UV-Vis (ϵ , M⁻¹ cm⁻¹): λ_{\max} (DMSO) = 279 (23529), 314 (12097), 327 (11331), 343 (8283). ¹H NMR (CDCl₃, 400.13 MHz, 298K) δ (ppm): 7.38 (td, J = 3.29, 1.59 Hz, 1H, H₇), 7.50–7.57 (m, 5H, H₉–H₁₁), 7.81 (dd, J = 9.0, 2.1 Hz, 1H, H₁), 7.90 (td, J = 7.7,

1.5 Hz, 1H, H₆), 8.09 (d, $J = 2.0$ Hz, 1H, H₂), 8.12 (d, $J = 9.0$ Hz, 1H, H₃), 8.55 (s, 1H, H₄), 8.68 (d, $J = 8.0$ Hz, 1H, H₅), 8.73 (d, $J = 4.4$ Hz, 1H, H₈). ¹³C {¹H} NMR (CDCl₃, 100.6 MHz, 298 K) δ (ppm): 120.02, 121.02, 121.88, 124.26, 127.99, 128.63, 128.72, 129.56, 131.91, 132.93, 137.02, 137.71, 147.10, 148.49, 149.23, 155.96. ¹H NMR (DMSO-d₆, 300 MHz, 298K) δ (ppm): 7.64 (m, 6H, H₇+H₉-H₁₁), 7.98 (m, 2H, H₁+H₂), 8.10 (td, $J = 6.0$ Hz, 3Hz, 1H, H₆), 8.17 (d, $J = 9.0$ Hz 1H, H₃), 8.52 (s, 1H, H₄), 8.68 (d, $J = 6$ Hz, 1H, H₅), 8.77 (d, $J = 6$ Hz, 1H, H₈). ESI-MS (CH₃CN): m/z (100%) = 363.32 [M+H]⁺ (calc. 363.05).

2.2.2. Synthesis of 4-(4-phenyl-2-(pyridin-2-yl)quinolin-6-yl)phenol (**2**)

3 g (8.31 mmol) of ligand **1** and 4-(tetrahydro-2H-pyran-2-yloxy) phenyl boronic acid (2.21 g, 9.97 mmol) were dissolved in 70 mL of degassed toluene under inert atmosphere, followed by the addition of K₂CO₃ (6.88 g, 49.86 mmol) and Pd(PPh₃)₄ (0.24g, 0.21 mmol) and the resulting mixture was refluxed for 3 days. The solution was then cooled to ambient temperature, filtered from filter paper and extracted with ethyl acetate and deionized water. The organic layer was dried over MgSO₄, filtered off and evaporated under reduced pressure before drying in a vacuum oven overnight affording 3.23 g of the intermediate **2-THP**. Yield: (85%). ¹H NMR (CDCl₃, 400.13 MHz, 298K) δ (ppm): 1.66–1.75 (m, 3H, H₁₅+H₁₆), 1.89 (m, 2H, H₁₇), 2.02 (sext, $J = 7.0$ Hz, 1H, H₁₅), 3.62 (dt, $J = 4.3, 3.0$ Hz, 1H, H₁₈), 3.92 (td, $J = 10.5, 3.1$ Hz, 1H, H₁₈), 5.47 (t, $J = 3.2$ Hz, 1H, H₁₄), 7.13 (d, $J = 4.9$ Hz, 2H, H₁₂), 7.36 (t, $J = 5.8$ Hz, 1H, H₇), 7.51–7.58 (m, 5H, H₉-H₁₁), 7.63 (d, $J = 6.3$ Hz, 2H, H₁₃), 7.90 (td, $J = 7.7, 1.8$ Hz, 1H, H₆), 7.98 (dd, $J = 8.8, 2.0$ Hz, 1H, H₁), 8.09 (d, $J = 2.0$ Hz, 1H, H₂), 8.29(d, $J = 8.7$ Hz, 1H, H₃), 8.52 (s, 1H, H₄), 8.70 (d, $J = 8.7$ Hz, 1H, H₅), 8.72 (d, $J = 4.8$ Hz, 1H, H₈).

Subsequently, the obtained solid **2-THP** was dissolved in THF (150 mL) and then concentrated HCl (2 mL) was added. The color of the mixture was immediately turned to an intense red and it was stirred at room temperature overnight under argon. After that period a yellow solid had precipitated. Solvents were removed under reduced pressure and the remaining solid was stirred in deionized water, filtered off, washed with deionized water and then the solid was dried under vacuum overnight. The obtained solid was redissolved in THF and was treated with 20 mL of an 0.5M aqueous solution of Na₂CO₃. The mixture was stirred at ambient temperature for 6 h and then

the organic solvent was removed under pressure. The obtained solid was washed extensively with deionized water, filtered off and dried under vacuum overnight. Yield: 96% (3.10 g). M.p.: 213.5–217.1 °C. *Anal.* Calc. for (2) × 1.0(H₂O), C₂₆H₂₀N₂O₂: C, 79.58; H, 5.14; N, 7.14. Found: C, 79.64; H, 4.55; N, 7.04%. IR (KBr, $\tilde{\nu}$ in cm⁻¹): 3423 (br, ν (OH)), 3056 (w, ν (C–H_{arom})), 2925 (w, ν (C–H_{aliph})), 1610 (vs), 1586 (vs), 1521 (s), 1490 (vs, ν (C=N)), 1438 (m), 1363 (m), 1273 (vs), 1260 (w, δ (O–H)), 1281 (s), 1176 (m, ν (C–O)), 1027 (w), 895 (w), 825 (vs), 797 (s), 760 (s), 702 (s), 620 (s), 590 (m), 543 (m), 529 (m), 440 (w). UV-Vis (ϵ , M⁻¹ cm⁻¹): λ_{\max} (DMSO) = 289 (34160), 343 (14460), 358 (14833). ¹H NMR (DMSO-d₆, 300 MHz, 298K) δ (ppm): 6.89 (d, J = 10.0 Hz, 2H, H₁₂), 7.50–7.68 (m, 6H, H₇+H₁₃+H₉–H₁₁), 8.00 (s, 1H, H₂), 8.04–8.11 (m, 2H, H₆+H₁), 8.24 (d, J = 8.0 Hz, 1H, H₃), 8.48 (s, 1H, H₄), 8.67 (d, J = 6.0 Hz, 1H, H₅), 8.73 (d, J = 6.0 Hz, 1H, H₈), 9.69 (s, 1H, –OH). ¹H NMR (CDCl₃, 400.13 MHz, 298K) δ (ppm): 5.04 (s, 1H, –OH), 6.91 (d, J = 8.4 Hz, 2H, H₁₂), 7.37 (t, J = 4.0 Hz, 1H, H₇), 7.51–7.57 (m, 5H, H₉–H₁₁), 7.63 (d, J = 7.6 Hz, 2H, H₁₃), 7.90 (t, J = 7.6 Hz, 1H, H₆), 7.97 (d, J = 8.8 Hz, 1H, H₁), 8.07 (s, 1H, H₂), 8.29 (d, J = 8.8 Hz, 1H, H₃), 8.52 (s, 1H, H₄), 8.70 (d, J = 7.6 Hz, 1H, H₅), 8.73 (d, J = 4.8 Hz, 1H, H₈). ¹³C {¹H} NMR (CDCl₃, 100.6 MHz, 298K) δ (ppm): 115.87, 119.71, 122.00, 122.49, 124.00, 126.60, 126.89, 128.27, 128.48, 128.56, 128.97, 129.58, 130.31, 131.98, 132.08, 132.60, 137.10, 138.25, 139.19, 147.48, 149.04, 149.31, 155.06, 156.00, 156.29. ESI-MS (CH₃CN) : m/z (100%) = 375.48 [M+H]⁺ (calc. 374.14), 397.46 [M+Na]⁺ (calc. 397.13).

2.2.3. Synthesis of *mer*-[Rh(1)Cl₃(CH₃OH)] (3)

Into a 50 mL round bottom flask, 56 mg (0.21 mmol) of RhCl₃×3H₂O was dissolved in 13 mL of warm CH₃OH giving a brown-red solution. An equimolar amount (77 mg) of **1** was dissolved in 13 mL of warm methanol and subsequently was added slowly and under stirring to the homogenous solution above. During the addition, the color of the solution changed to bright orange and the solution was heated to a gentle reflux for about 1 h. Upon cooling at ambient temperature a yellow-orange microcrystalline solid was precipitated and was dried *in vacuo* affording 71 mg of analytically pure complex **3** (yield: 55.4%). The clear orange filtrate was left to stand in a closed vial at ambient temperature, affording needle-like orange crystals suitable for single crystal X-ray diffraction study after a period of two weeks. The crystals were

collected from the mother liquor and were dried *in vacuo* affording a further crop of the desired product (27 mg). Total yield: Yield: 77% (98 mg). *Anal. Calc.* for (3) \times 1.0(H₂O), C₂₁H₁₉BrCl₃N₂O₂Rh: C, 40.62; H, 3.09; N, 4.50. Found: C, 40.34; H, 3.00; N, 4.70%. IR (KBr, $\tilde{\nu}$ in cm⁻¹): 3065 (w, ν (C–H_{arom})), 1591 (m), 1540 (m), 1481 (vs), 1437 (m), 1383 (s), 1361 (w), 1261 (w), 1221 (w), 1165 (m), 1130 (w), 1075 (w), 985 (w), 886 (m), 827 (w), 785 (s), 756 (m), 698 (m), 646 (w), 601 (w), 544 (w). UV-Vis (ϵ , M⁻¹ cm⁻¹): λ_{\max} (DMSO) = 297 (28829), 342 (15196), 355 (19291), 398 (3367). ¹H NMR (DMSO-d₆, 300 MHz, 298K) δ (ppm): 3.17 (s, 3H, CH₃), 4.08 (br.s, 1H, –OH), 7.69–7.77 (m, 5H, H₉–H₁₁), 7.88 (t, J = 6 Hz, 1H, H₇), 8.03 (s, 1H, H₂), 8.24 (d, J = 6 Hz, 1H, H₁), 8.32 (t, J = 6 Hz, 1H, H₆), 8.75 (s, 1H, H₄), 8.96 (d, J = 6 Hz, 1H, H₃), 9.62 (d, J = 9 Hz, 1H, H₅), 9.81 (d, J = 6 Hz, 1H, H₈).

2.2.4. Synthesis of *mer*-[Rh(2)Cl₃(CH₃OH)] (4)

In a 50 mL round bottom flask, 54 mg (0.205 mmol) of RhCl₃ \times 3H₂O was dissolved in 5 mL of warm CH₃OH. An equimolar amount (77 mg) of **2** dissolved in warm CH₃OH (10 mL) was added under stirring to the homogenous red-brown solution and the mixture was then heated under reflux for about 1 h affording an orange solution. After cooling at room temperature, the clear solution was left for slow evaporation at room temperature. Two days later, orange needle-like crystals were formed and some of them were suitable for single-crystal X-ray diffraction study. The rest of the crystalline material was collected by filtration and dried *in vacuo* affording 30 mg (yield: 40%) of **4**. A further amount of the compound was collected upon slow evaporation of the mother liquor at ambient temperature. Total yield: 60% (45 mg). *Anal. Calc.* for Calc. for for (1) \times 3(H₂O), C₂₇H₂₈Cl₃N₂O₅Rh: C, 48.40; H, 4.22; N, 4.18%. Found: C, 48.68; H, 3.87; N, 4.37%. *Calc. IR* (KBr, $\tilde{\nu}$ in cm⁻¹): 3334 (br, ν (OH)), 1605 (s), 1588 (s), 1520 (m), 1488 (vs), 1443 (w), 1385 (m), 1359 (m), 1259 (w, δ (O–H)), 1180 (m, ν (C–O)), 1131 (w), 1110 (w), 894 (w), 873 (w), 826 (s), 782 (s), 760 (s), 704 (s), 629 (w), 604 (w), 529 (w). UV-Vis (ϵ , M⁻¹ cm⁻¹): λ_{\max} (DMSO) = 312 (47186), 367 (13246), 392 (18466), 426 (12073). ¹H NMR (DMSO-d₆, 300 MHz, 298K) δ (ppm): 3.17 (s, 3H, CH₃), 4.08 (br, 1H, –OH), 6.92 (d, J = 9 Hz, 2H, H₁₂), 7.59 (d, J = 6 Hz, 2H, H₁₃), 7.69–7.83 (m, 6H, H₇+ H₉–H₁₁), 8.01 (s, 1H, H₂), 8.27–8.37 (m, 2H,

H₁+H₆), 8.67 (s, 1H, H₄), 8.93 (d, *J* = 9 Hz, 1H, H₃), 9.70 (d, *J* = 9 Hz, 1H, H₅), 9.80 (br.s, 1H, H₈), 9.83 (br.s, 1H, –OH of –PhOH).

2.3. X-ray analysis

The data collections were performed on a Bruker D8-Venture (**3**), a Nonius Kappa CCD (**2**, **4**), and a Bruker X8-KappaApexII diffractometer by using Cu-*K*α- (**1**, $\lambda = 1.54178 \text{ \AA}$) or Mo-*K*α radiation ($\lambda = 0.7103 \text{ \AA}$), generated by a sealed tube. The diffractometers were equipped with a low-temperature device; the measurements were performed at 123(2) K.

Intensities were measured by fine-slicing ω and φ -scans and corrected for background, polarization, absorption and Lorentz effects [30].

The structures were solved by intrinsic phasing methods implemented in Sheldrick's XT program and refined anisotropically by the least-square procedure implemented in the SHELX program system [31,32]. Hydrogen atoms were included using the riding model on the bound carbon atoms.

Crystallographic data and refinement conditions for compounds **1–4** are summarized in Table 1.

Table 1

Crystal and refinement data for **1**, **2**·HCl·H₂O, **3**·2CH₃OH and **4**.

	1	2 ·HCl·H ₂ O	3 ·2CH ₃ OH	4
Empirical formula	C ₂₀ H ₁₃ BrN ₂	C ₂₆ H ₂₁ ClN ₂ O ₂	C ₂₃ H ₂₅ BrCl ₃ N ₂ O ₃ Rh	C ₂₇ H ₂₂ Cl ₃ N ₂ O ₂ Rh
Molecular weight	361.23	428.90	666.62	615.72
Crystal color	colourless	yellow	orange	orange
Crystal size (mm ³)	0.30×0.08×0.02	0.24 × 0.12×0.11	0.24×0.10×0.06	0.34×0.10×0.07
<i>T</i> (K)	123(2)	123(2)	123(2)	123(2)
Crystal system	orthorhombic	orthorhombic	monoclinic	trigonal
Space group	<i>Pbca</i>	<i>Pbca</i>	<i>P2₁/c</i>	<i>P3₂21</i>
<i>Unit cell dimensions</i>				
α (°)	8.0304(3)	17.3460(3)	14.1125(4)	28.2138(12)
β (°)	19.3245(7)	10.1900(2)	13.9370(3)	28.2138(12)
γ (°)	19.4156(7)	23.7866(5)	27.7042(8)	8.4237(4)

α (°)	90	90	90	90
β (°)	90	90	111.344(2)	90
γ (°)	90	90	90	120
V (Å ³)	3018.57(19)	4204.42(14)	5075.3(2)	5807.1(6)
Z	8	8	8	6
ρ_{calc} (g cm ⁻³)	1.590	1.355	1.745	1.056
μ (mm ⁻¹)	3.698(Cu-K α)	0.208(Mo-K α)	2.592(Mo-K α)	0.667(Mo-K α)
$F(000)$	1456.0	1792	2656	1860
2θ range (°)	9.09 to 134.96	2.35 to 28.00	5.468 to 52	3.334 to 58.408
Reflections collected	11737	59408	23710	59766
Unique reflections	2626	5077	9729	9983
Parameters refined	0/208	0/292	6/611	88/376
R_1 [$I > 2\sigma(I)$]	0.0616	0.0406	0.0425	0.0465
wR_2 (all data)	0.1748	0.1250	0.0943	0.1229
Goodness-of-fit on F^2	1.029	1.062	1.089	1.050
Largest diff. peak/hole (e Å ⁻³)	0.76/−2.01	0.624/−0.369	0.59/−0.60	1.28/−0.61

2.4. Biological experiments

The biological experiments PAF- induced platelet aggregation, and the inhibitory effect of the synthetic compounds) were performed according to well described protocols [1,14]. Briefly, for the washed rabbit platelets (WRPs) preparation, rabbit platelets (platelet rich plasma), were washed on Ficoll-Paque cushions and adjusted to 2.5×10^8 platelets/ml of Tyrode's buffer, pH 7.2. The dilution of PAF was prepared in pyrogen-free 0.15 M NaCl containing 2.5 mg/ml of crystallized bovine serum albumin, required for dispersion of PAF. The compounds under investigation were first dissolved in DMSO and aliquots of these solutions were then added in solutions (2.5 mg BSA/mL) of saline. Microliters of the dilution of PAF (final concentration, 10^{-10} M, in the cuvette) were added in the cuvette of the aggregometer and calculate the height of the platelet aggregation. The inhibitory effect of the rhodium precursor $\text{RhCl}_3 \cdot 3\text{H}_2\text{O}$, the ligands and the rhodium(III) coordination compounds prepared, towards the washed rabbit platelets (WRPs) aggregation experiments, was carried out by literature methods [15]. The aggregometer was from Chrono-Log Corporation, (Haverton, PA). Bovine serum albumin (BSA), PAF and analytical solvents for the biological assays were purchased from Sigma. The measurements were repeated at least twice for each sample concentration in three different WRPs preparations, in order to

ensure reproducibility. All experiments were also followed by appropriate control tests of the solvent used (saline solution of BSA, DMSO aliquots in a saline solution of BSA-2.5 mg BSA/mL saline- or just in saline), in WRPs.

3. Results and Discussion

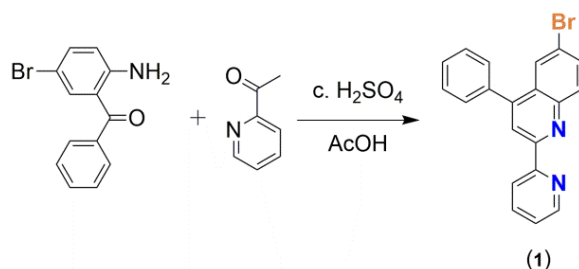
3.1. Synthesis and characterization of the organic ligands 1–2

Compound **1** was prepared in 86% yield following a Friedländer condensation reaction of 2-amino-5-bromobenzophenone (otherwise known as (2-amino-5-bromophenyl)phenyl-methanone) and 2-acetylpyridine under acidic condition. The synthetic procedure is outlined in Scheme 3. Although this ligand has been employed in previous studies for the preparation of 6-(4-vinylphenyl)-2-(2-pyridine)-4-phenylquinoline employed as a monomer in radical polymerizations, as well as for the synthesis of 6-(9-carbazolyl)-4-phenyl-2-(2-pyridyl)-quinoline [25], its synthetic protocol and spectroscopic characterization were not reported up to now [33,34].

A complete spectroscopic characterization of **1** is now included supported by mass spectrometric methods. The electrospray mass spectrum of **1** exhibits a base peak at m/z 363.32 for the $[M+H]^+$ ion with an isotope pattern characteristic of the presence of one bromine atom and is depicted in the supporting information (Fig. S1).

The ^1H and ^{13}C NMR spectra of **1** in CDCl_3 display the number of expected resonances (Figs. S2,S3). The characteristic down field doublet resonances for the H_8 and H_5 protons of the pyridine ring are observed at δ 8.77 and δ 8.68 respectively, while the singlet resonance at δ 8.52 is due to the H_4 proton of the benzene ring of 6-Br-quinoline.

In the FT-IR spectrum quite informative is the very strong stretching vibration for the ν (C-Br) symmetric mode at 1116 cm^{-1} .



Scheme 3. Synthesis of 6-bromo-2-(2-pyridine)-4-phenylquinoline (**1**).

Suitable colorless single crystals of **1** were obtained upon slow evaporation of a DMSO- d_6 solution of the compound at ambient temperature. The molecular structure of **1** is shown in Fig. 1.

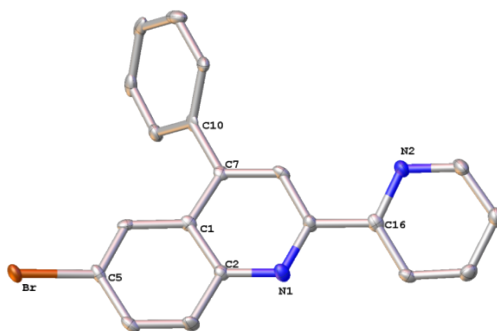
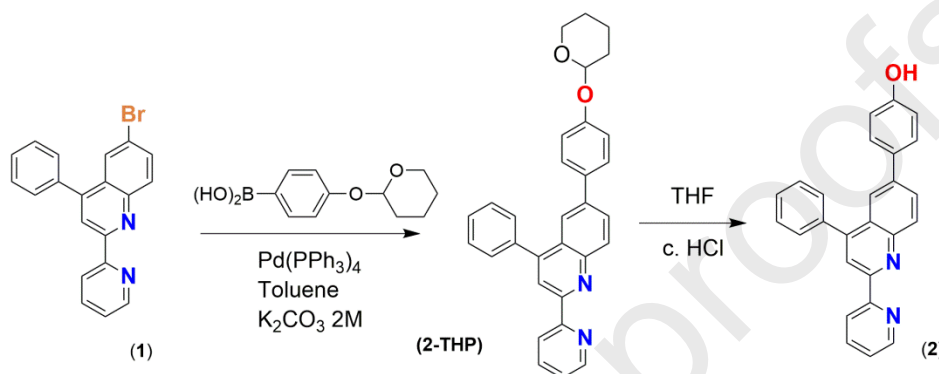


Fig. 1. The molecular structure of **1**. Hydrogen atoms are omitted for clarity. The ellipsoids were plotted at 50% probability. Selected bond lengths (Å) and angles (°): Br–C5 = 1.906(4), N1–C2 = 1.365(5), N1–C9 = 1.324(5), C9–C16 = 1.488(5), N2–C16 = 1.353(5), N2–C17 = 1.341(5), N1–C9–C16 = 117.2(4), C8–C7–C10 = 120.2(4).

Compound **1** crystallizes in the orthorhombic *Pbca* space group and as expected, the two nitrogen atoms of the bipyridine group of the ligand adopt a *trans*-configuration. The pyridine ring close to the quinoline ring deviates from planarity (angle between the least square planes of rings containing atoms N1 and N2 is 19.62°). The phenyl group connected to C7 is also deviating from planarity (angle between the least square planes of rings containing atoms N1 and C10 is 57.62°) and is further involved in typical intramolecular C–H \cdots π contacts [35] with the phenyl ring (C10–C15) from an adjacent molecule (distance of (C11–H11 \cdots centroid) = 2.917 Å). In the crystal packing of **1** the bromine atom displays weak C–H \cdots Br contacts (C8–H8 \cdots Br = 3.889 Å, H8 \cdots Br = 3.262 Å; C18–H18 \cdots Br = 3.875 Å, H18 \cdots Br = 3.244 Å) that is in accord with the literature [36]. Finally the crystal is stabilized by rather weak π – π stacking interactions between the phenyl and pyridine ring (distance between centroids (C1–C6) and (N1–C1–C9) of 3.962 Å) as shown in the supporting information (Fig. S4) [37].

The analytically pure compound **1** obtained through the route described previously, was further used for the synthesis of the hydroxylphenyl functionalized ligand **2**, in a two-step reaction as presented in Scheme 4. The first step leads to the isolation of the

tetrahydropyran (THP)-protected intermediate **2-THP**, through the Suzuki coupling of **1** with the 4-(tetrahydro-2H-pyran-2-yloxy) phenyl boronic acid using Pd(PPh₃)₄ as catalyst. The purity of this intermediate was checked by ¹H NMR in CDCl₃ (Fig. S5a) proving the successful formation of the **2-THP** derivative which was used without any further purification. Subsequent removal of the tetrahydropyranyl protective group under acidic conditions, led to the desired ligand **2** in 96% yield (Fig. S5b).



Scheme 4. Synthesis of 6-(4-yl-phenol)-2-(2-pyridine)-4-phenylquinoline (**2**).

The molecular composition of **2** was unambiguously confirmed by electrospray mass spectrometry (Fig. S6) exhibiting peaks at m/z 375.48 and 397.46 corresponding to $[M+H]^+$ (basic peak) and $[M+Na]^+$. The ¹H and ¹³C NMR spectra of **2** in DMSO-*d*₆, are presented in the supporting information (Figs. S7,S8). The low field single resonance of the phenolic hydroxyl proton is observed at δ 9.69. An important feature in the ¹H NMR spectrum of **2** is the presence of the single resonance at δ 8.48 that is characteristic of the H₄ proton of the ligand. The doublet resonances at δ 6.89 and δ 7.52 are typical for the H₁₂ and H₁₃ protons of the -PhOH group. The latter (doublet resonance for H₁₃) is overlapped with the resonance signal of H₇ and the protons of the phenyl group (H₉-H₁₁) respectively. All other resonances appear in the expected region; their assignment was based on a ¹H-¹H COSY NMR spectrum, confirming undoubtedly the molecular structure of **2**.

Despite repeated crystal growth attempts with this compound only microcrystals or powders were obtained. Therefore we tried with the protonated form of the ligand (**2**·HCl), that is the compound obtained prior to treatment with Na₂CO_{3(aq)} (see experimental). The IR and ¹H NMR spectra of **2**·HCl that was used for crystallization,

are included in the supporting information (Figs. S9,S10). Finally, yellow single crystals of $2 \cdot \text{HCl} \cdot \text{H}_2\text{O}$ suitable for single-crystal X-ray diffraction studies, were obtained upon slow diffusion of diisopropyl ether to a methanol solution of $2 \cdot \text{HCl}$ at ambient temperature.

Compound $2 \cdot \text{HCl} \cdot \text{H}_2\text{O}$ is crystallizing in the orthorhombic crystallographic system, $Pbca$ space group and the molecular structure is depicted in Fig. 2.

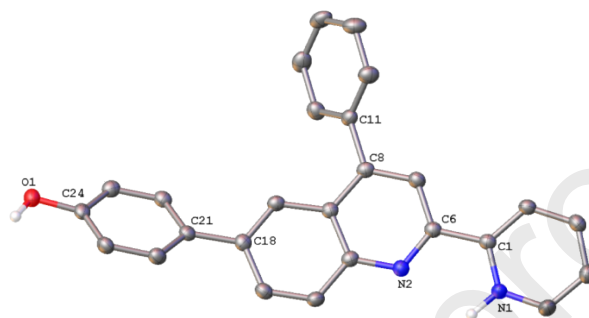


Fig. 2. The molecular structure of $2 \cdot \text{HCl} \cdot \text{H}_2\text{O}$. Cl counter anion and the crystalline water molecule are omitted for clarity. The ellipsoids were plotted at 50% probability. Selected bond lengths (Å) and angles (°): O1–H14 = 0.97(2), O1–C24 = 1.3621(18), N1–C1 = 1.3560(19), N1–H1A = 0.941(18), N2–C6 = 1.3306(18), N2–C10 = 1.3558(19), C5–N1–C1 = 123.00(13), C5–N1–H1A = 120.4(11), N2–C6–C1 = 115.45(12), N2–C10–C20 = 118.03(4).

The phenyl substituent on C8 is twisted out of the plane of the bipyridine (bpy) moiety (angles between the least square planes of rings containing N1, N2 and C11–C16 are 49.77°). Also the phenol group on C18 deviates from planarity (angles between the least square planes of rings containing C18, C21 are 36.0°). In the bipyridine moiety the two nitrogen atoms about the biaryl bond are in the *cis*-position and this preference could be attributed to the intramolecular hydrogen bonding of N2 to the adjacent H1A of the N1 atom (N1–H1A \cdots N2 = 2.217 Å, bond angle = 106.76°) [38].

The packing in the crystal is such that four sets of ribbons (eight molecules) are stabilized by weak intermolecular π – π stacking (distance between centroids are in the range of 3.927 to 4.024 Å). Each set of ribbons is almost orthogonal to one another. The phenolic oxygen atom of the ligand displays non classical intermolecular hydrogen

bonding interactions with an adjacent molecule, (distance of $O1\cdots H5A-C5 = 2.497 \text{ \AA}$ (N1 ring); bond angle of 125.63°) [39] and characteristic $O1-H1\cdots\pi$ weak hydrogen bonding interactions at a distance of 3.402 \AA ($O1-H1\cdots$ centroid (ring N1)) that overall stabilize the structure in the crystal [40]. The network that is formed is reinforced by intermolecular hydrogen bonding interactions between the oxygen atoms of the phenol group with solvated water molecules ($O2_{\text{water}}$) in the lattice ($O1-H1\cdots O2_{\text{water}} = 2.699 \text{ \AA}$) and the Cl counter ions ($O2-H2B\cdots Cl = 2.433 \text{ \AA}$) respectively. Overall these interactions are shown in the supporting information (Fig. S11).

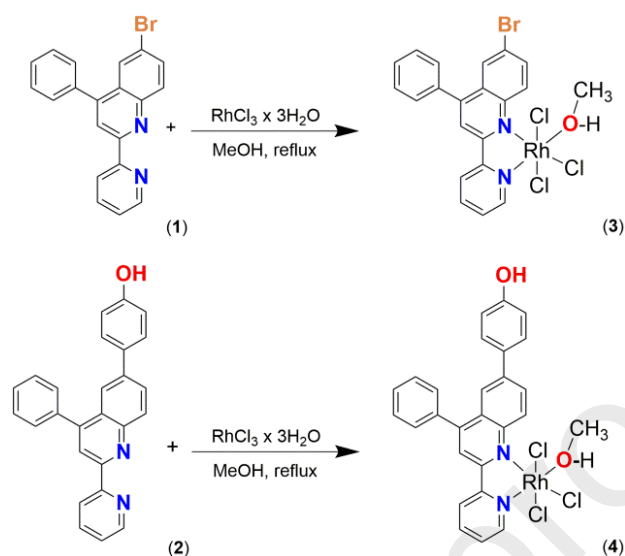
Although $2 \cdot HCl \cdot H_2O$ is the structure of the protonated form of the ligand precursor **2**, the information collected upon structure elucidation is of importance in relation to the nature of the ligand. In addition, a Cambridge Crystallographic Database search revealed that its crystal structure has not been reported previously, while crystallographic data on this class of compounds are quite rare. So far, only the molecular structures of 2-(2-Pyridyl)-4-phenyl-quinoline and of its relevant complex with Zn(II) have been reported [25].

Finally it should be mentioned, that **1**, **2** are easily prepared materials, in high yields and in a multi-gram scale which can be stored for weeks to months in common desiccators. Accordingly they can be potentially used as building blocks for the synthesis of a number of coordination compounds, as is the case herein for the Rh(III) coordination compounds **3** and **4** respectively.

3.2. Synthesis and characterization of the rhodium(III) complexes **3–4**

The octahedral rhodium(III) complexes **3** and **4** were prepared according to the synthetic protocol described previously by our group [15]. The reaction of $RhCl_3 \cdot 3H_2O$ with an equimolar amount of **1** or **2** was taken place in hot methanol (Scheme 5). Subsequent work up of the reaction mixture resulted to the isolation of analytically pure *mer*- $[Rh(\mathbf{1})Cl_3(CH_3OH)]$ (**3**) and *mer*- $[Rh(\mathbf{2})Cl_3(CH_3OH)]$ (**4**) as yellow-brown (**3**) and orange (**4**) microcrystalline solids in 77% and 60% yield respectively. The structures of **3** and **4**, as the *mer* isomers, was undoubtedly confirmed from a single crystal X-ray diffraction analysis performed (vide infra). Complex **3** is soluble in methanol, acetone,

CH₃CN, THF, DMF and DMSO, while **4** dissolves in acetone, methanol, DMF and DMSO. Both compounds are sparingly soluble in water.



Scheme 5. The synthetic procedure of the rhodium(III) complexes **3** and **4**.

The IR spectrum of **3** in the region of 1600–400 cm⁻¹ exhibits strong bands for the C=C, C=N stretching vibrations and the pyridyl ring deformation bands of **1**. The presence of a medium intensity band at 1130 cm⁻¹ could be presumably attributed to the ν (C–Br) symmetric mode.

The ¹H NMR spectrum of **3** recorded in DMSO-d₆, is consistent with the presence of a single ligand environment (Fig. S12). Assignment of the proton resonances became apparent with the help of a ¹H–¹H COSY NMR experiment performed. Coordination of **1** has been identified unambiguously by the pronounced downfield shift of the H₈ and H₅ protons at δ 9.81 and δ 9.62, in comparison to the corresponding resonance signals of the free ligand at δ 8.77 and δ 8.68 respectively ($\Delta\delta = 1.04$ and 0.94 ppm).¹ In addition, the double resonance found for the H₃ proton at δ 8.96 is shifted towards lower fields by 0.79 ppm as compared to that of **1**, while the multiplet

¹ A detailed comparison with the NMR data of the free ligand (in the same solvent) cannot be made. Single crystal X-ray diffraction studies and ¹H-NMR studies for **3** have shown that the free ligand exists in a *trans* conformation. Upon coordination to a metal center the *cis* conformation is adopted.

resonances observed at δ 8.32 and δ 7.88 are assigned to the adjacent H₆ and H₇ protons. In the aliphatic region, only two resonances were observed at δ 3.17 (–CH₃) and δ 4.088 (–OH) that can be attributed to free methanol [41].

In the IR spectrum of **4** characteristic is a broad vibration for the ν (O–H) of the phenol group at 3334 cm⁻¹ that is typical for the intermolecular hydrogen bonded –OH stretch. The δ (O–H) bending vibration probably occurs at 1259 cm⁻¹ and the ν (C–O) stretching mode is present as a medium intensity band at 1179 cm⁻¹.

The solution ¹H NMR spectrum of **4** (crystals of **4** dissolved in DMSO-d₆) in the aromatic region displays sharp, well resolved and intense resonances that are characteristics for the presence of **2** (Fig. S13). Ligand coordination becomes evident by the remarkable low frequency shift of the signals due to H₈ (δ 9.80) and H₅ (δ 9.70). In the free ligand, these resonance signals are at δ 8.73 and δ 8.67 respectively. According to the ¹H–¹H COSY NMR spectrum, the singlet resonance at δ 9.80 is overlapped with a rather broad resonance signal at δ 9.83 that is attributed to the phenolic hydroxyl proton (–OH). In addition, the doublet resonance for H₃ (δ 8.93) is downfield shifted when compared to that of compound **2** at δ 8.24 ($\Delta\delta$ = 0.69 ppm), denoting that the coordination environment around it has been altered significantly. The H₆ and H₁ protons appear as a multiplet resonance between 8.27–8.37 ppm, while the H₇ resonance at δ 7.69–7.83 is overlapped with the phenyl group protons H₉–H₁₁. In the aliphatic region of the ¹H NMR spectrum of complex **4**, only the presence of free methanol was detected at δ 3.17 (–CH₃) and δ 4.08 (–OH), as reported previously for the analogues complex **3**.

3.3. Thermal behavior of complexes **3–4**

Thermal stability of **3**, **4** (in the crystalline form) was examined by means of a thermogravimetric analysis (TGA) performed in the temperature range 25–800 °C under nitrogen atmosphere (Figs. S14,S15). The thermal analysis data of the rhodium(III) complexes indicate that, decomposition starts at 25 °C and the first weight loss (128.2 °C for **3**; temperature range 25–105 °C for **4**) corresponds to loss of one coordinated methanol molecule (Obs. 6.0 and 5.5%, Calcd. 5.3 and 5.3 % for **3** and **4** respectively).

For complex **3** a detailed analysis could not be undertaken since thermal decomposition continues over 800 °C. Weight losses cannot be assigned to individual moieties and thus the information provided is rather limited. On the other hand, complex **4** continues to decompose thermally, up to 800 °C through a second plateau (between 128 °C–265 °C) and intermediate non-well separated steps. Attribution of weight losses to individual molecule moieties is not possible for any of these steps. However, the total weight loss (75.56 %) from 125 °C to 800 °C could be assigned to loss of the C₂₆H₁₇NO₂Cl₃ moiety, that corresponds to the fragment [(**2**)Cl₃] (Calcd. 78.03%). At 800 °C, the total weight loss of 18.9 % corresponds to Rh₂O₃ (Calcd. 20.26 %).

3.4. Structural characterization of complexes **3–4**

The solid-state structures of the rhodium(III) complexes **3**·2CH₃OH and **4** were determined by single-crystal X-ray diffraction. Orange needle-like crystals of **3**·2CH₃OH were grown upon standing of a methanol solution of the complex in a closed vial at ambient temperature over a period of two weeks. This compound is crystallizing in the monoclinic crystallographic system, *P*2₁/*c* space group. The molecular structure of **3** is presented in Fig. 3 and selected bond distances and angles are listed in Table 2. Two independent molecules of **3**·2CH₃OH with slightly different bonding parameters were found in the asymmetric unit. Complex **3** shows a distorted octahedral geometry with three chlorido ligands in the *mer* configuration and the ligand **1** coordinated in a bidentate fashion. The remaining site of the coordination sphere is completed by a methanol molecule bound to each rhodium(III) center. The Rh(1)–O(1) bond length of the coordinated methanol molecule is at 2.080(3) Å and the C(21)–O(1)–Rh(1) angle at 124.1(3)°. Typical bond angles around the metal center (one of the two independent molecules) manifesting distortion, are these of Cl(3)–Rh(1)–Cl(1) = 89.63(5)°, O(1)–Rh(1)–Cl(1) = 93.23(11)°, O(1)–Rh(1)–Cl(3) = 84.86(10)° and Cl(2)–Rh(1)–Cl(1) = 178.58(4)° respectively. The Rh(1)–N(2) bond distance of 1.987(4) Å is significantly shorter compared to that of Rh(1)–N(1) = 2.084 Å(4), reported for the *mer*-[RhCl₃(bpy)(CH₃OH)]·CH₃OH complex [41]. The bond lengths of Rh(1)–Cl(1) =

2.338(14) Å, Rh(1)–Cl(2) = 2.334(13) Å and Rh(1)–Cl(3) = 2.326(13) Å compare well with the values reported for other rhodium(III) complexes [42].

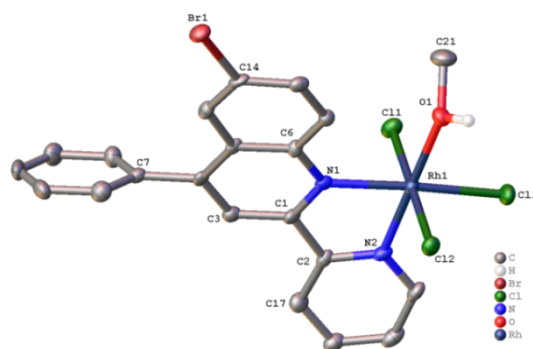


Fig. 3. Molecular structure of **3** (one of the two molecules in the crystal). Hydrogen atoms and solvated methanol molecules are omitted for clarity. The ellipsoids were plotted at 50% probability.

The molecular structure of **3** is stabilized by intermolecular O–H \cdots O and O–H \cdots Cl hydrogen bonding interactions. Coordinated and free methanol molecules participate in these interactions (Fig. S16), while selected hydrogen bonding interactions are shown in the supporting information (Table S1). For example, the O(5)–H(5) \cdots Cl(4)) hydrogen bonding interaction of 2.525 Å (bond angle (\angle) O–H \cdots Cl = 147.7 $^\circ$) compares well with the one reported for the *fac*-trichloridotris(trimethylphosphane- κP)rhodium(III) methanol hemihydrate, (O–H \cdots Cl bonding interaction of 2.57 Å (bond angle (\angle) O–H \cdots Cl = 157 $^\circ$) [43]. Complex **3** exhibits characteristic C–H \cdots π interactions (Fig. S17) that overall stabilize the structure in the crystal (distance of (C21–H21C) \cdots centroid (ring C(28)) = 3.650 Å and that of (C42–H42B) \cdots centroid (ring C(7)) = 3.239 Å).

Table 2

Selected bond lengths (Å) and bond angles ($^\circ$) for **3**·2CH₃OH and **4**.

bond lengths		bond angles	
3 ·2CH ₃ OH ^a			
Rh(1)–Cl(1)	2.3383(14)	Cl(2)–Rh(1)–Cl(1)	178.58(4)
Rh(1)–Cl(2)	2.3336(13)	Cl(3)–Rh(1)–Cl(1)	89.63(5)
Rh(1)–Cl(3)	2.3261(13)	Cl(3)–Rh(1)–Cl(2)	89.99(5)
Rh(1)–N(1)	2.084(4)	O(1)–Rh(1)–Cl(1)	93.23(11)

Rh(1)–N(2)	1.987(4)	O(1)–Rh(1)–Cl(2)	88.09(11)
Rh(1)–O(1)	2.080(3)	O(1)–Rh(1)–Cl(3)	84.86(10)
C(14)–Br(1)	1.899(4)	O(1)–Rh(1)–N(1)	99.41(14)
N(1)–C(1)	1.333(6)	N(1)–Rh(1)–Cl(1)	89.14(11)
N(1)–C(6)	1.387(6)	N(1)–Rh(1)–Cl(3)	175.62(11)
O(1)–C(21)	1.433(7)	C(21)–O(1)–Rh(1)	124.10(3)
4			
Rh–Cl(1)	2.3387(14)	Cl(2)–Rh–Cl(3)	178.48(5)
Rh–Cl(2)	2.3225(14)	Cl(2)–Rh–Cl(1)	91.10(6)
Rh–Cl(3)	2.3533(15)	Cl(1)–Rh–Cl(3)	90.42(6)
Rh–N(1)	1.974(4)	O(2)–Rh–Cl(1)	87.13(12)
Rh–N(2)	2.041(4)	O(2)–Rh–Cl(2)	91.64(14)
Rh–O(2)	2.106(4)	O(2)–Rh–Cl(3)	88.38(14)
N(1)–C(1)	1.346(6)	O(2)–Rh–N(1)	177.03(19)
N(1)–C(5)	1.339(7)	N(1)–Rh–Cl(1)	95.26 (12)
O(2)–C(27)	1.461(10)	N(1)–Rh–Cl(3)	89.83(12)
O(1)–C(24)	1.364(6)	C(27)–O(2)–Rh	122.2(4)

^a Bond lengths and angles of one of the two independent molecules.

Finally, the crystal packing in the structure of **3** is such that symmetry related molecules are separated by typical π – π stacking interactions at a distance of 3.596 Å and 3.844 Å respectively (Fig. 4).

Although rhodium(III) complexes with coordinated solvent molecules have been reported [44,45,46], the number of crystallographically characterized methanol solvate complexes is quite rare. A crystallographic search in the Cambridge Structural Database revealed only the *mer*-[Rh(L¹)Cl₃(CH₃OH)] (L¹ = 2-(2'-pyridyl)quinoxaline) [16] and the *mer*-[Rh(bpy)Cl₃(CH₃OH)]·(CH₃OH) [41] complexes respectively.

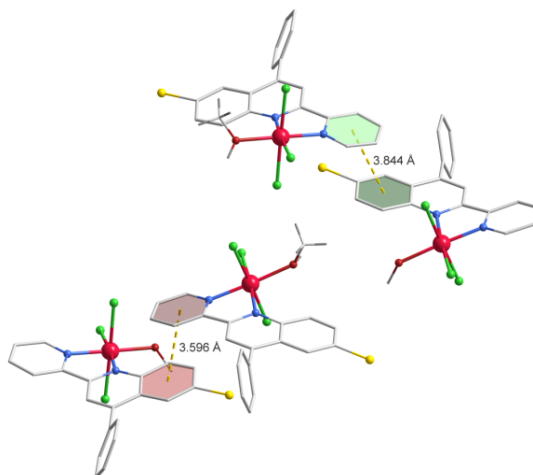


Fig. 4. Intermolecular π - π stacking interactions in complex **3**. Carbon, gray; hydrogen, light gray; nitrogen, blue; bromine, yellow; chlorine, green; oxygen, brown-red; rhodium, red.

Orange needle-like crystals of **4** were grown upon slow evaporation of the mother liquor (CH_3OH) at ambient temperature over a period of two days. Compound **4** is crystallizing in the trigonal crystallographic system, $P3_221$ space group and the molecular structure of **4** is presented in Fig. 5.

The coordination geometry is that of a distorted octahedron and the ligands around the rhodium(III) center are in the *mer* configuration. In complex **4**, the Rh-O(2) bond length of the coordinated methanol is at 2.110(4) Å and compares well with that reported for complex **3**. In addition, the Rh-N(1) and Rh-N(2) bond distances are at 1.974(4) Å and at 2.041 (4) Å respectively.

Moreover, it should be mentioned that the phenyl ring involving the atoms C15 to C20 is disordered over two distinct positions in the ratio 1:1. This side occupancy is omitted for clarity. Selected bond lengths and angles for complex **4** are listed in Table 2.

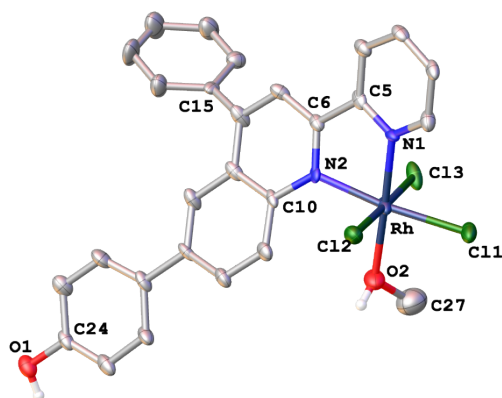


Fig. 5. Molecular structure of **4**. Hydrogen atoms are omitted for clarity. The ellipsoids were plotted at 50% probability.

In the crystal structure of **4** pair of molecules display intermolecular π - π stacking interactions between the quinoline and phenyl rings of symmetry related molecules (distance between centroids of 3.604 Å and 3.611 Å). The dimeric subunits of **4** form long chains that are separated by a π - π stacking at a distance of 3.475 Å (Fig. 6). These are connected each other with typical O(1)-H(1)···Cl(3) hydrogen bonding interactions at a distance of 3.197 (4) Å and a bond angle of 148.7°.

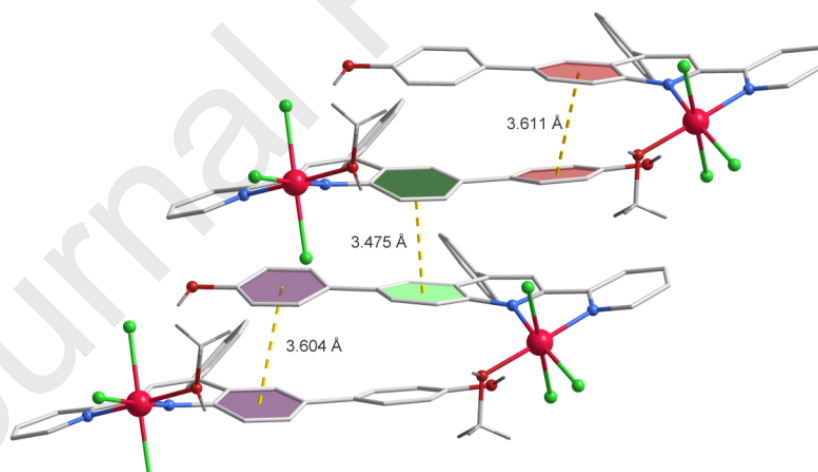


Fig. 6. Intermolecular π - π stacking interactions in complex **4**. Carbon, gray; hydrogen, light gray; nitrogen, blue; bromine, yellow; chlorine, green; oxygen, brown-red; rhodium, red.

3.5. Electronic spectra

The solution absorption spectra of the organic ligands **1**, **2** and the complexes **3**, **4** in DMSO are depicted in the supporting information (Fig. S18a). The intense high

energy bands at 279 nm for **1** and at 289 nm for **2** are assigned to π - π^* transitions. For **2**, the bands centered at 343 and 358 nm are red shifted as compared to the -Br derivative **1** (bands at 327, 343 nm), apparently due to the hydroxyphenyl group that acts as a better π -donor.

The electronic spectra of **3** and **4** display typical metal to ligand charge transfer bands (MLCT) at 342 nm and 355 nm for **3**, while for complex **4** a rather broad MLCT band centered at 392 nm with shoulders at 367 nm and 426 nm respectively, is observed. Furthermore the spectra were recorded within the concentration range of 10^{-4} to 10^{-6} M (**3**) and 10^{-5} to 10^{-7} M (**4**), without changes in the spectral shape (Figs. S18b,c) and the Lambert-Beer law is obeyed (linear correlation between absorption and concentration). These results imply the absence of inter- or intra-molecular π - π interactions in solution [47].

Complexes **3** and **4** are stable in DMSO solution, over a period of 24 h. No new peaks or isosbestic points were observed (Figs. S19,S20). For complex **4**, the absorption spectrum shows a slow decrease of the band intensities without shifting of the absorption maxima. This could be explained on the basis of progressive aggregation that leads to a decrease of the complex concentration [48].

3.6. Solution stability of **3** and **4** by ^1H NMR spectroscopy

For the biological evaluation of this class of compounds their stability in the required medium is a prerequisite. DMSO is a very common solvent used for this purposes, and its coordination ability to the relevant metal center via either S or O atoms has been well documented in the literature [46,49,50,51]. Complexes **3**, **4** were dissolved in DMSO- d_6 solution at room temperature and their stability was monitored by ^1H NMR spectroscopy, without exposure to direct light, over a period of 24 to 48 h. In fact, no new signals were observed in the aromatic region (Fig. S21 (**3**), Fig. S22 (**4**)). Therefore, complexes **3** and **4** can be potentially used for the proposed biological evaluation in this medium. Monitoring of the ^1H NMR spectra of **3**, **4** for a longer period of time in the absence of light, reveals that slow isomerization to equilibrium mixtures of the *mer* (**3**, **4**) and the *fac* (**3a**, **4a**) isomers takes place. In fact **3/3a** (36/64) and **4/4a** (50:50) isomers were formed after 9 and 5 days respectively in DMSO- d_6 solution at

room temperature. This is in accord to the remarks of Sheldrick et al. on the structurally related complexes *mer*-[RhCl₃L(DMSO)] (L = dpq, dppn), where a 92:8 *mer/fac* ratio was found for L = dpq after 4 days [52].

3.7. Biological evaluation

Herein, we report for the first time on the biological study of the organic precursors **1** and **2** and the corresponding octahedral rhodium(III) complexes **3** and **4**, emphasizing on the evaluation of the anti-platelet activity expressed.

Precursors and Rh Complexes	IC ₅₀ (μM) towards PAF (10 ⁻¹⁰ M, in the cuvette) in WRPs	SD	reference
<i>Ligands</i>			
1	3.4	0.2	this work
2	4.4	0.2	this work
L	6.4	0.5	[20]
L ¹	32	15	[14,18]
<i>Starting materials</i>			
RhCl ₃ ×3H ₂ O	67	22	[14]
<i>Complexes</i>			

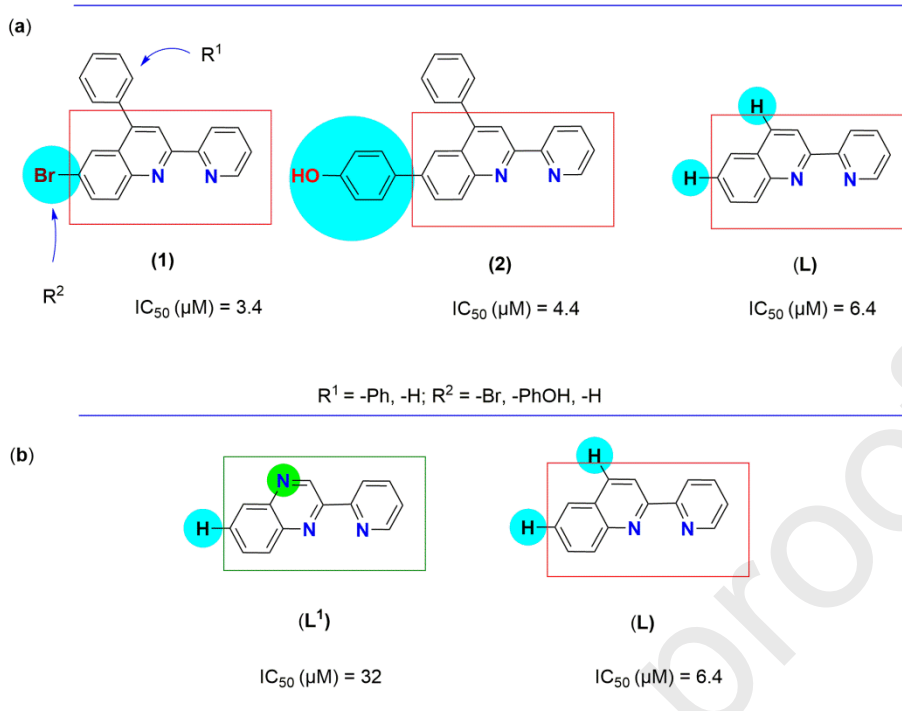
<i>mer</i> -[Rh(L)Cl ₃ (CH ₃ OH)]	2.6	2.0	[14]
(3)	1.0	0.6	this work
(4)	3.9	0.2	this work

The new substances were biologically evaluated towards PAF induced activities in washed rabbit platelets (WRPs) aggregation assays. PAF is a link of an increasing list of mediators implicated in physiological as well as pathological inflammatory processes, since it has the ability to stimulate inflammatory cells and to mediate both cell-cell interactions and intracellular signaling. On the other hand, PAF-inhibitors have also anti-inflammatory activity [53]. In fact, the anti-inflammatory action of the new compounds may be exerted by their interaction with PAFR, blocking the PAFR activation. The inhibitory effect of all the compounds tested, including the rhodium precursor RhCl₃×H₂O, was expressed by their IC₅₀ value in μM as presented in Table

3. Table 3

Inhibition of PAF induced aggregation by the rhodium(III) coordination compounds, the ligands and the rhodium precursor toward WRPs

The IC₅₀ values reflect the inhibition strength of each compound, since a low IC₅₀ value reveals stronger inhibition of the PAF-induced aggregation for a given concentration. As far as the biological behavior of the organic ligands is concerned, valuable information is obtained upon comparison of the structurally related compounds **1** and **2** with the organic precursor 2-(2'-pyridyl)quinoline (**L**) [20], that served as a control compound (Scheme 6).



Scheme 6. Comparison of the organic precursors presented in this work, displaying (a) pyridyl-quinoline or (b) pyridyl-quinoxaline core.

From this scheme it is evident that **1**, **2** and **L**, all display the typical pyridyl-quinoline core, differing however on the nature of the R^1 , R^2 substituents. Both **1** and **2** have the same functional group R^1 at the quinolinic part of the common core ($R^1 = -\text{Ph}$), as opposed to the R^2 substituent that changes from **1** ($R^2 = -\text{Br}$) to **2** ($R^2 = -\text{PhOH}$) respectively. On the other hand, the less sterically demanding ligand **L** contains the same R^1 , R^2 groups ($R^1 = R^2 = \text{H}$).

The results listed in Table 3 clearly show that within the organic precursors tested, **1** is the most potent inhibitor. In fact, the IC_{50} value drops from 6.4 μM (**L**) to 4.4 μM (**2**) and to 3.4 μM (**1**) respectively. It seems therefore that for this class of compounds, the inhibitory effect against the PAF induced aggregation (anti-PAF activity) is affected but to different extends by the presence of the R^1 and R^2 substituents. Presumably the presence of the bulky $R^2 = -\text{PhOH}$ group, may be responsible for the weaker inhibitory effect of **2** as compared to **1**.

On the other hand, a plausible explanation about the less pronounced inhibitory effect of **L**¹ = 2-(2'-pyridyl)quinoxaline [15], in comparison to that of **L**, could be made

according to the aforementioned manner (Scheme 6b). From the obtained experimental data, it is obvious that the inhibitory effect of **L**¹, comprising the quinoxaline moiety, is reduced almost five times on going to **L** that holds the quinolinic functional group. In fact, the IC₅₀ drops from 32 μM (**L**¹) to 6.4 μM (**L**) respectively. The data (IC₅₀ values in Table 3) also suggest that, in the case of PAF-induced WRP aggregation, the octahedral rhodium(III) complexes **3**, **4** exhibit a biological activity in the micromolar range with IC₅₀ values of 1 μM and 3.9 μM respectively. This is in agreement with the inhibitory effect reported (IC₅₀ = 2.6 μM) for the structurally related *mer*-[Rh(**L**¹)Cl₃(CH₃OH)] complex [15].

Upon a careful examination of the results listed above we further noticed, that coordination of **1** to the rhodium(III) metal center, enhances the inhibitory potency against the PAF-induced aggregation (synergetic effect). In fact, on going from **1** (3.4 μM) to **3** (1.0 μM) the PAF inhibitory effect increases approximately by a factor of three, (the IC₅₀ value decreases) rendering compound **3** more potent against PAF inhibition. Complex **4** incorporating the bulkier organic precursor **2** shows a slightly higher inhibitory activity (IC₅₀ = 3.9 μM) than that of **2** (IC₅₀ = 4.4 μM). From these findings one may propose that the biological activity of **4** and of the organic precursor **2** practically remains unaltered. In any case, the combination of the rhodium precursor RhCl₃×3H₂O (IC₅₀ = 67 μM) and **1** or **2** affording **3** and **4** (synergetic effect), leads to a dramatic increase of the inhibitory activity against the PAF-induced aggregation. Conclusively the inhibitory activity against PAF decreases in the following order: **3** > **1** > **4** > **2**.

From the library of more than 30 metal-based inhibitors created so far [3,17], we have realized that this effect (synergetic effect), is a general trend which is followed in the present case as well. These results underline the substantial role of the final structure of the proposed metal-based inhibitor. On the other hand, it should be noted that parameters such as the total charge on the metal complex cannot be excluded [54]. The neutral character of the rhodium(III) complexes **3**, **4** is a feature that may affect permeability through cell membranes and needs further investigation [55].

Notably the IC₅₀ values of the title compounds **3**, **4** are comparable or even better than the inhibitory effect of Gingolides, a class of natural specific inhibitors from the leaves and roots of the Chinese tree *Gingo biloba*. This becomes evident within the

series of Gingolides BN 52020 ($IC_{50} = 3.6 \mu\text{M}$), BN 52021 ($IC_{50} = 9.7 \mu\text{M}$) and BN 52022 ($IC_{50} = 38 \mu\text{M}$) respectively [56]. This is of particular interest denoting the great potency of the present compounds, as possible anti-inflammatory agents in the future, provided that they display the required pharmacological profile (toxicity evaluation etc.). According to Leung, Ma and co-workers [10] this field is still immature and very promising, aiming to produce a series of metal complexes that could be approved in the treatment of inflammatory diseases.

Although the biological probe studied in this report is a complicated system, we managed to confirm the preliminary structure-activity relationships established [3,17] and as a result to increase the number of metal-based inhibitors of PAF (compounds with anti-platelet potency) in the library of metal complexes that has been created. Finally, the results of this study will help us to rational design new compounds with improved anti-PAF activity. To reinforce our experimental findings further studies are required, and towards this goal work is currently underway.

4. Conclusions

In conclusion, we have successfully synthesized and characterized two new substituted pyridyl-quinoline ligands (**1**, **2**) that served as potent building blocks for the synthesis of the octahedral rhodium(III) complexes (**3**, **4**). The biological evaluation of the new compounds **1–4** towards the PAF-induced aggregation in washed rabbit platelets (WRPs) is also reported, revealing that all substances display potent activities. Complex **3** bearing the less sterically demanding ligand **1** is a better inhibitor of PAF as compared to complex **4**. In total **3** and **4** are potent inhibitors of PAF in the micromolar range ($IC_{50} = 1.0 \mu\text{M}$ to $3.4 \mu\text{M}$).

Notably it can be pointed out that the established structure-activity relationships from our previously reported studies are followed as well, for this type of metal complexes (same trend). Thus the nature of both the metal center and of the organic ligand, contribute substantially to the biological action expressed (synergetic effect). Moreover the size of the metal complex, determines the extent of their inhibitory action.

Conclusively, the new substances could be successfully added to the existing library of more than 30 small molecules with potent anti-PAF activity. Accordingly, these findings would enable us to estimate or even to predict the anti-PAF activity of

other metal-based complexes with analogous molecular structures. Based on the fact that PAF is a potent mediator of inflammation, inhibition of its biological activity by metal-based inhibitors, could contribute to the development of new metal-based agents that may have anti-inflammatory potency.

Finally, the information obtained from the present report, provides us with the required knowledge in an effort to obtain more efficacious anti-PAF agents that could be used as anti-inflammatory and anti-cancer drugs in the future.

Acknowledgements

A.I. Philippopoulos would like to thank Prof. Dr. A.C. Filippou of the Chemistry Department of the University of Bonn for the elemental analyses performed. Mrs. C. Rhode of the Chemistry Department of the University of Bonn (Department of x-Ray Crystallography) is highly acknowledged for the X-ray measurements. A.I. Philippopoulos would like to thank «The Special Research Account of the National and Kapodistrian University of Athens», for financial support (Research grant No.15653).

Appendix A. Supplementary data

CCDC 1969013, 1969014, 1969016 and 1969015 contains the supplementary crystallographic data for **1**, **2**·HCl·H₂O, **3**·2CH₃OH and **4**. These data can be obtained free of charge via <http://www.ccdc.cam.ac.uk/conts/retrieving.html>, or from the Cambridge Crystallographic Data Centre, 12 Union Road, Cambridge CB2 1EZ, UK; fax: (+44) 1223-336-033; or e-mail: deposit@ccdc.cam.ac.uk.

Supplementary data include selected spectroscopic and structural characterization data of compounds **1–4**.

References

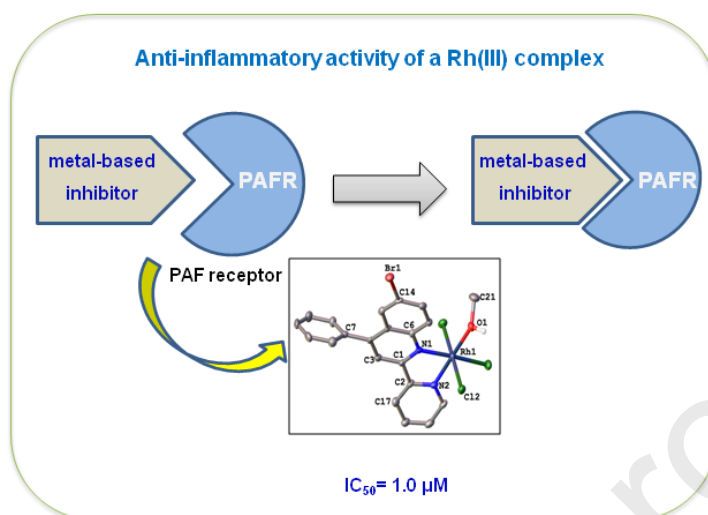
- [1] C.A. Demopoulos, R.N Pinckard, D.J. Hanahan, *J. Biol. Chem.* 254 (1979) 9355.
- [2] S. Antonopoulou, T. Nomikos, H.C Karantonis, E. Fragopoulou, C.A Demopoulos "PAF, a potent lipid mediator". In: *Bioactive Phospholipids. Role*

- in inflammation and Atherosclerosis. Edited by Tselepis AD. 1st ed. Kerala, India: Transworld Research Network; 2008. pp. 85–134.
- [3] V.D. Papakonstantinou, N. Lagopati, E.C. Tsilibary, C.A. Demopoulos, A.I. Philippopoulos, *Bioinorganic Chemistry and Applications*, vol. 2017, Article ID 6947034, 19 pages, 2017, <https://doi.org/10.1155/2017/6947034>.
- [4] J.B. Summers, D.H. Albert, *Adv. Pharmacol.* 32 (1995) 67.
- [5] E. Koch, *Phytomedicine* 12 (2005) 10.
- [6] I. Izquierdo, M. Merlos, J. Garc'ia-Rafanell, *Drugs Today* 39 (2003) 451.
- [7] P. Singh, I-N. Singh, S-C. Mondal, L. Singh, V-K. Garg, *Fitoterapia* 84 (2013) 180.
- [8] T.W. Hambley, *Science* 318 (2007) 1392.
- [9] E. Meggers, *Current Opinion in Chemical Biology* 11 (2007) 287.
- [10] C-H. Leung, S. Li, H-J. Zhong, D-L. Ma, *Chem. Sci.* 6 (2015) 871.
- [11] (a) L. Salassa, *Eur. J. Inorg. Chem.* (2011) 4931; (b) A. de Almeida, B.L. Oliveira, J.D.G. Correia, G. Soveral, A. Casini, *Coord. Chem. Rev.* 257 (2013) 2689.
- [12] A. Bergamo, G. Sava, *Dalton Trans.* 40 (2011) 7817.
- [13] S.H. van Rijt, P.J. Sadler, *Drug Discovery Today* 14 (2009) 1089-.
- [14] A.I. Philippopoulos, N. Tsantila, C.A. Demopoulos, C.P. Raptopoulou, V. Likodimos, P. Falaras, *Polyhedron* 28 (2009) 3310.
- [15] A.B. Tsoupras, A. Papakyriakou, C.A. Demopoulos, A.I. Philippopoulos, *J. Inorg. Biochem.* 120 (2013) 63.
- [16] P. Falaras, A.I. Philippopoulos, "Platelet Activating Factor (PAF) inhibitors with possible antitumor activity", Industrial Property Organization of Greece, 2009, patent number 1006959.
- [17] A. Peppas, A. Kalabalidis, V.D. Papakonstantinou, C.A. Demopoulos, G. Schnakenburg, A.I. Philippopoulos, "Rhodium-based Inhibitors of the Platelet Activating Factor (PAF). A new class of potent anti-inflammatory drugs", Book chapter in: *Chemical Elements (Fluorine, Rhodium and Rubidium). Properties, Synthesis and Applications*. Editor. A. Huff. Nova Science Publishers, New York 2018, pages 127–169.

- [18] M. Prokopi, "Ir(I) and Ir(III) complexes and study of their biological activity against the Platelet Activating Factor", Master thesis, National and Kapodistrian University of Athens, Athens, Greece, 2015.
- [19] A-B. Tsoupras, V. Papakonstantinou, G.M. Stamatakis, C.A. Demopoulos, P. Falaras, A.I. Philippopoulos, *Sci. Lett. J.* 4 (2015) 208.
- [20] A. Siabali, "Ru(II) complexes and study of their biological activity against the Platelet Activating Factor", Master thesis, National and Kapodistrian University of Athens, Athens, Greece, 2015.
- [21] I.K. Hyland, R.F. O'Toole, J.A. Smith, A.C. Bissember, *ChemMedChem.* 13 (2018) 1873.
- [22] E. Sioriki, R. Lordan, F. Nahra, K. Van Hecke, I. Zabetakis, S.P. Nolan, *ChemMedChem.* 13 (2018) 2484.
- [23] (a) S. Campagna, A. Memmo, J.K. Stille, *J. Chem. Soc., Dalton Trans.* (1991) 2545; (b) G.C. Vougioukalakis, T. Stergiopoulos, A.G. Kontos, E.K. Pefkianakis, K. Papadopoulos, P. Falaras, *Dalton Trans.* 42 (2013) 6582.
- [24] E.M. Laguna, P.M. Olsen, M.D. Sterling, J.F. Eicher, A.L. Rheingold, C.H. Larsen, *Inorg. Chem.* 53 (2014) 12231.
- [25] X. Chen, D. Qiu, L. Ma, Y. Cheng, Y. Geng, Z. Xie, L. Wang, *Transition Met. Chem.* 31 (2006) 639.
- [26] P.D. Sybert, W.H. Beever, J.K. Stille, *Macromolecules* 14 (1981) 493.
- [27] R.B. Davis, L.C. Pizzini, *J. Org. Chem.* 25 (1960) 1884.
- [28] A.K. Andreopoulou, J.K. Kallitsis, *Macromolecules* 35 (2002) 5808.
- [29] D.R. Coulson, *Inorg. Synth.* 13 (1972) 121.
- [30] Bruker SADABS-2014/5 (Bruker AXS Karlsruhe; 2014).
- [31] G.M. Sheldrick *Acta Cryst.* A71 (2008) 3.
- [32] G.M. Sheldrick *Acta Cryst.* C71 (2008) 3.
- [33] S.N. Kourkouli, A. Siokou, A.A. Stefopoulos, F. Ravani, T. Plocke, M. Muller, J. Maultzsch, C. Thomsen, K. Papagelis, J.K. Kallitsis, *Macromolecules* 46 (2013) 2590.
- [34] A. Moutsiopoulou, K.A Andreopoulou, G. Lainioti, G. Bokias, G. Voyiatzis, J.K. Kallitsis. *Sens. Actuators B Chem.* 211 (2015) 235.
- [35] M. Nishio, *Cryst. Eng. Comm.* 6 (2004) 130.

- [36] C. Weck, F. Katzsch, T. Gruber, *J. Mol. Struct.* 1098 (2015) 261.
- [37] C. Janiak, *J. Chem. Soc., Dalton Trans.* (2000) 3885.
- [38] T. Steiner, *Angew. Chem. Int. Ed.* 41 (2002) 49.
- [39] G.R. Desiraju, *Acc. Chem. Res.* 24 (1991) 290.
- [40] M.A. Viswamitra, R. Radhakrishnan, J. Bandekar, G.R. Desiraju, *J. Am. Chem. Soc.* 115 (1993) 4868.
- [41] R. Bieda, I. Ott, M. Dobroschke, R. Gust, W.S. Sheldrick, *J. Inorg. Biochem.* 103 (2009) 698.
- [42] A. Dikhtiarenko, L. Torre-Fernández, S. García-Granda, J.R. García, J. Gimeno, *Acta Cryst. E*68 (2012) m713.
- [43] J.S. Merola, M.A. Franks, *Acta Cryst. E*71 (2015) m226.
- [44] A. Albinati, Urs E. Bucher, V. Gramlich, O. Renn, H. Rügger, L.M. Venanzi, *Inorg. Chim. Acta* 284 (1999) 191.
- [45] M.H. Zaghai, H.A. Qaseer, *Transition Met. Chem.* 16 (1991) 39.
- [46] U. Śliwińska-Hill, F.P. Pruchnik, I. Pelińska, S. Ułaszewski, A. Wilczok, A. Zajdel, *J. Inorg. Biochem.* 102 (2008) 1947.
- [47] J. Wang, A. Kulago, W.R. Browne, B.L. Feringa, *J. Am. Chem. Soc.* 132 (2010) 4191.
- [48] F. Battistin, F. Scaletti, G. Balducci, S. Pillozzi, A. Arcangeli, L. Messori, E. Alessio, *J. Inorg. Biochem.* 160 (2016) 180.
- [49] B.R. James, R.H. Morris, *Can. J. Chem.* 58 (1980) 399.
- [50] I. Ferrer, J. Rich, X. Fontrodona, M. Rodriguez, I. Romero, *Dalton Trans.* 42 (2013) 13461.
- [51] I. Bratsos, D. Urankar, E. Zanrando, P. Genova-Kalou, J. Košmirj, E. Alessio, I. Turel, *Dalton Trans.* 40 (2011) 5188.
- [52] Y. Geldmacher, M. Oleszak, W.S. Sheldrick, *Inorg. Chim. Acta* 393 (2012) 84.
- [53] R. Lordan, A. Tsoupras, I. Zabetakis, C.A. Demopoulos, *Molecules* 24 (2019) 4414.
- [54] C.N. Verani, *J. Inorg. Biochem.* 106 (2012) 59.
- [55] M. Harlos, I. Ott, R. Gust, H. Alborzina, S. Wölfl, A. Kromm, W.S. Sheldrick, *J. Med. Chem.* 51 (2008) 3924.
- [56] V.D. Papakonstantinou, *Hellenic Journal of Atherosclerosis*, 4 (2013) 109.

Journal Pre-proofs



Graphical Abstract Synopsis

Two octahedral rhodium(III) complexes incorporating new substituted pyridine-quinoline ligands were synthesized and structurally characterized. Biological studies demonstrate that the new complexes are potent anti-platelet agents in the micro-molar scale, owing to their potency to inhibit the action of PAF (Platelet-Activating Factor). This is an approach of continuous interest for the development of metal complexes with possible anti-inflammatory activity.

Highlights

- ▶ Synthesis and characterization of the substituted 2-(2'-Pyridyl)quinoline ligands **1**, **2**
- ▶ Structural characterization of *mer*-[RhCl₃(**1**)(CH₃OH)] (**3**) and *mer*-[RhCl₃(**2**)(CH₃OH)] (**4**)
- ▶ Complexes **3** and **4** are potent inhibitors of PAF in the micromolar scale
- ▶ **3** and **4** are possible anti-inflammatory agents